NASA Technical Memorandum 83296

APPLICATION OF A TRANSONIC POTENTIAL FLOW CODE TO THE STATIC AEROELASTIC ANALYSIS OF THREE-DIMENSIONAL WINGS

WOODROW WHITLOW, JR. AND ROBERT M. BENNETT

APRIL 1982

NASA

National Aeronautics and
Space Administration

Langley Research Center
Hampton, Virginia 23665

APPLICATION OF A TRANSONIC POTENTIAL FLOW CODE TO THE
STATIC AEROELASTIC ANALYSIS OF THREE-DIMENSIONAL WINGS

Woodrow Whitlow, Jr. and Robert M. Bennett
NASA Langley Research Center
Hampton, Virginia

Abstract

A method for including elastic effects in steady, transonic wing analysis is presented. Since the aerodynamic theory is nonlinear, the method requires the coupling of two iterative processes - an aerodynamic analysis and a structural analysis. A full potential analysis code, FLO22, is combined with a linear structural analysis to yield aerodynamic load distributions on and deflections of elastic wings. This method was used to analyze an aeroelastically-scaled wind tunnel model of a proposed executive-jet transport wing and an aeroelastic research wing. The results are compared with the corresponding rigid-wing analyses, and some effects of elasticity on the aerodynamic loading are noted.

Nomenclature

a	local speed of sound
b	wing span
c	local chord
C	influence function; deflection at (x,y) due to a unit load at (ξ, η)
C^{zz}	deflection at y due to a unit load at η
$C^{\theta\theta}$	angular rotation at y due to a unit moment at η
c_l	section lift coefficient
C_L	wing lift coefficient
C_M	wing pitching moment coefficient
C_p	pressure coefficient
ΔC_p	lifting pressure coefficient
F	lifting load element
h	wing deflection
m	twisting moment about elastic axis
M	Mach number
q	dynamic pressure
u,v,w	velocities, normalized with respect to free stream speed, in the x,y and z directions, respectively
x,ξ	streamwise coordinate
$\bar{x},\bar{\xi}$	coordinate perpendicular to elastic axis
y,η	spanwise coordinate
$\bar{y},\bar{\eta}$	coordinate along elastic axis
z	coordinate normal to x-y plane
α	wing root angle-of-attack
γ	ratio of specific heats
θ	streamwise twist angle
ϕ	velocity potential
ω	relaxation factor

Introduction

Methods for predicting transonic aerodynamic loads on wings have been developed assuming complete wing rigidity.[1-3] In reality, airplane wings are flexible and, as is commonly known, experience deflections that may significantly alter their loading. Thus, accurate prediction of aerodynamic loads on flexible wings and proper interpretation of experimental data require consideration of the effects of elasticity on these loads.

When the flow field is described by linear equations, aeroelastically-corrected loads can be easily determined by direct solution of a set of matrix equations relating angle-of-attack, dynamic pressure, and structural and aerodynamic influence coefficients.[4] For example, Pai and Sears[5] used matrix methods to calculate lift distributions on swept, flexible wings and demonstrated some effects of sweep on aeroelastic phenomena. The FLEXSTAB program[6] represents the state-of-the-art in methods for computing aerodynamic loads on elastic wings.

At transonic speeds, however, such direct methods are not yet developed. Alternative methods include correcting calculations made using matrix methods with empirical relationships derived from experimental transonic data[7] and using deflected wing shapes measured during wind tunnel tests in transonic analysis codes.[8] Since these methods require supporting experimental data, they are quite limited in their application.

Chipman et al.[9] developed a procedure for including elastic effects in transonic load predictions that requires no experimental data. That procedure iterates between a transonic small disturbance method and a linear structural approximation that models wings as slender beams. Using not-fully-converged aerodynamic loads, deflections and rotations of streamwise strips of wings are calculated and used to define new wing shapes. Those shapes are then used in the aerodynamic computations, and the process is repeated until a converged aerodynamic solution and wing shape are obtained. The choice of a beam structural model limits the method to the analysis of high-aspect-ratio wings with chordwise rigidity. Also, as the authors note, for some supercritical Mach numbers, small disturbance theory may predict shock waves at incorrect locations, causing moments and calculated twist angles to be in error. These points suggest the need for a more accurate aerodynamic theory and a more general structural representation.

This paper presents an improved method, based on full potential aerodynamics, for calculating steady, transonic loads on flexible wings. The present method also iterates between a nonconverged aerodynamic calculation and a linear structural analysis. Since, the aerodynamic analysis is based on full potential theory, calculated moments and related twists should be more accurate than those obtained

with small disturbance aerodynamic loads.
Assuming linear structural relationships and
hence small wing deflections, the structural
analysis employs an influence coefficient method
which can be used without the slender beam
assumptions. In computing deflections,
distributed loads are represented as a network
of discrete loads located at the centroids of
corresponding area elements. Representing the
loads in this manner allows wing deflections to
be computed directly at the load points without
the beam assumptions. The present method can,
of course, be used for beam analysis as a
particular case. To demonstrate the present
method, aerodynamic loads on an
aeroelastically-scaled wind tunnel model of a
proposed executive-jet transport wing[10] and on
an aeroelastic research wing[11] have been
computed. Since bending and torsional
stiffnesses along the elastic axis were
available for these wings, slender beam theory
was used for the structural analyses of the
wings studied in this paper. The results of
those analyses are presented and compared with
corresponding rigid-wing analyses and measured
data.

Aerodynamic Analysis

Aerodynamic solutions are computed numeri-
cally using the FLO22 computer program[2] which
solves the full potential equation

$$(a^2-u^2)\phi_{xx} + (a^2-v^2)\phi_{yy} + (a^2-w^2)\phi_{zz}$$

$$-2(uv\phi_{xy} + uw\phi_{xz} + vw\phi_{yz}) = 0 \qquad (1)$$

where a is the local speed of sound,
and $(u,v,w) = (\phi_x, \phi_y, \phi_z)$ are the local
components of velocity normalized with respect
to the free stream speed. Equation (1) is
solved, using a nonconservative finite
difference procedure, on a sequence of
successively finer grids. This procedure is
computationally more efficient than using a
single fine grid.

For the results presented in this paper,
the initial grid was chosen to have 48, 8, and 8
points in the x, y, and z directions,
respectively, and was eventually refined to 192
x 32 x 32. The results presented herein were
obtained on the finest grid. All aerodynamic
computations were performed on a Control Data
Corporation (CDC) CYBER 203 using a partially
vectorized version of FLO22. Nondimensional
pressure distributions, C_p, were then obtained
from the following expression

$$C_p = \frac{2}{\gamma M^2} \left\{ \left[1 + \frac{(\gamma-1)}{2} M^2(1-(u^2+v^2+w^2)) \right]^{\frac{\gamma}{\gamma-1}} -1 \right\}$$
$$(2)$$

It should be noted that FLO22 cannot be used to
calculate the effects of fuselage interference
on wing loading.

Structural Analysis

For a given load distribution, $\Delta p(x,y)$,
wing deflections, $h(x,y)$, can be obtained from

$$h(x,y) = \iint C(x,y;\xi,\eta)\Delta p(\xi,\eta)d\xi d\eta \qquad (3)$$

where the flexibility influence function,
$C(x,y;\xi,\eta)$, defines the deflection at (x,y) due
to a unit load at (ξ,η). Since the elastic pro-
perties of a typical wing are generally very
complicated, it is usually not possible to
derive analytic expressions for influence func-
tions. Thus, it is usually necessary to deter-
mine numerical values of C at specific locations
on the wing. In the present analysis, load
distributions obtained by solving (1) are
represented as a network of load elements
(discrete forces) concentrated at the centroids
of the areas as shown in figure 1. Deflections,
$\{h\}$, at those points can then be expressed as

$$\{h\} = [C]\{F\} \qquad (4)$$

where $F_i = (\Delta p \Delta \xi \Delta \eta)_i$ is the force applied at
the centroid of the ith area element.

An important advantage of representing the
distributed load as a network of discrete forces
is that it allows the structural analysis to be
performed without the slender beam assumptions.
That is, given an influence coefficient matrix,
deflections at the load points can be computed
directly from (4). This means that low-aspect-
ratio wings, which generally cannot be modeled
as slender beams, may be analyzed using the pre-
sent method. The structural influence coeffi-
cient matrix, C, can be determined, for example,
using a finite element structural analysis or by
experiment. However, because linear structural
relationships are used, the present analysis is
limited to cases where the wing deflections are
small.

For the applications presented in this
paper, the wings were of high aspect-ratio and
in the present analysis were treated as slender
beams. The beam analysis requires the defini-
tion of an elastic axis and distributions along
the elastic axis of stiffnesses in bending (EI),
torsion (GJ), and shearing (GK). Each load
element is represented as a force at the elastic
axis and a moment about the elastic axis (see
figure 2). For slender beams, the influence
function can be written as

$$C(\bar{x},\bar{y};\bar{\xi},\bar{\eta}) = C^{zz}(\bar{y},\bar{\eta}) + \bar{x}C^{\theta\theta}(\bar{y},\bar{\eta}) \qquad (5)$$

where C^{zz} is the vertical deflection at $\bar{y}$ due
to a unit load at $\bar{\eta}$, and $C^{\theta\theta}$ is the angular
rotation of a strip normal to the elastic axis
at $\bar{y}$ due to a unit moment at $\bar{\eta}$. C^{zz} and
$C^{\theta\theta}$ are derived from the following expressions
given in chapter two of reference 1

$$C^{zz}(\bar{y},\bar{\eta}) = \int_0^{\bar{y}} \frac{(\bar{\eta}-\lambda)(\bar{y}-\lambda)}{EI} d\bar{\lambda} + \int_0^{\bar{y}} \frac{d\bar{\lambda}}{GK} \quad (\bar{\eta} \geq \bar{y})$$

$$C^{zz}(\bar{y},\bar{\eta}) = \int_0^{\bar{\eta}} \frac{(\bar{\eta}-\lambda)(\bar{y}-\lambda)}{EI} d\bar{\lambda} + \int_0^{\bar{\eta}} \frac{d\bar{\lambda}}{GK} \quad (\bar{\eta} \leq \bar{y})$$
$$(6)$$

$$c^{\theta\theta}(\bar{y},\bar{n}) = \int_0^{\bar{y}} \frac{d\bar{\lambda}}{GJ} \quad (\bar{n}\geq\bar{y})$$

$$c^{\theta\theta}(\bar{y},\bar{n}) = \int_0^{\bar{n}} \frac{d\bar{\lambda}}{GJ} \quad (\bar{n}\leq\bar{y}) \qquad (7)$$

where $\bar{\lambda}$ is a dummy variable of integration, and the coordinate system is defined in figure 2. GK distributions were not available for the wings analyzed in this study, therefore shearing effects were not included in C^{zz}. Since (6) and (7) are used to derive C^{zz} and $C^{\theta\theta}$ along the elastic axis, the structural influence coefficient matrices can be chosen to have a desired number of elements which in the present analysis is equal to the number of load elements. Using the beam theory assumptions, deflections, $\{h\}$, at the locations of the load elements are given by

$$\{h\} = [C^{zz}]\{F\} + \lceil\bar{x}_i\rfloor [C^{\theta\theta}]\{m\} \qquad (8)$$

where $m_i = \bar{\xi}_i F_i$ is the twisting moment about the elastic axis associated with each load element. Equation (8) is valid only for wings that can be modeled as slender beams and thus is a special case of (4).

The deflection calculation is performed external to FLO22, on a CDC CYBER 175, and is iterated as the aerodynamic load is updated (typically, deflections are computed after each 20-25 iterations of the aerodynamic solution). Since the aerodynamic calculation is itself iterative, the two iterations are converged concurrently (see figure 3). It is relatively straightforward to include the deflection and aerodynamic load calculations in a single code, but the present procedure allows periodic examination of the intermediate solution. The cost of a converged flexible-wing calculation is not a great deal more than that of corresponding rigid-wing computations. This is because a not-fully-converged aerodynamic solution is used for each deflection calculation and the computation of deflections requires relatively few computer resources.

At the nth structural iteration, intermediate deflections are computed from (8) and new deflections determined using the relaxation formula[9]

$$\{h\}^{n+1} = \{h\}^n + \omega(\{h\} - \{h\}^n) \qquad (9)$$

where $\{h\}$ represents the intermediate deflections. In this study the deflections were always underrelaxed ($\omega=0.75$). The relaxed deflections are added to the original wing coordinates to obtain a new wing shape and the iterative solution of (1) by FLO22 is continued. As in reference 9, this process (figure 3) is repeated until a converged aerodynamic solution and wing shape are obtained. In this study, solutions were considered converged when ϕ

changed by less than 2×10^{-5} between aerodynamic iterations and all wing deflections changed by less than two percent between structural iterations.

The calculations were performed subject to one of the following conditions: (1) wing root angle-of-attack (α) specified and the resulting loads and deflections calculated or (2) wing lift coefficient (C_L) specified and the required root angle-of-attack determined during the calculations. In the latter case, because FLO22 has no provision for specifying lift, necessary adjustments in angle-of-attack were made at each structural interaction until the solution converged to the desired lift.

Applications

The present method has been used to calculate loads and deflections for a wind tunnel flutter model of a proposed executive-jet-transport wing[10] and for the DAST (Drones for Aerodynamic and Structural Testing) ARW-2 (Aeroelastic Research Wing Number 2).[11] The planforms of these wings are shown in figure 4. For the transport wing model, some comparisons of calculated and measured tip deflections and twist angles are shown. While influence coefficents were not measured for either wing, EI and GJ distributions were available. Therefore, beam theory was used for the structural analyses of these high-aspect-ratio wings.

For use in the deflection calcuations, pressure distributions obtained from FLO22 were represented as a network of 200 discrete load elements with 10 elements per chord at 20 locations on the semispan. Equation (8) was then used to compute deflections at each load element location. On the CYBER 175, two times as many load elements per span location could have been used, at little extra cost, with the calculations still accomplished in memory.

Transport Wing Model

The transport wing model, which had supercritical airfoil sections, was a 1/6.5 scale flutter model of a proposed executive-jet transport wing and was designed for Mach number (M) of 0.82 and dynamic pressure (q) of 30 psf. It was constructed of fiberglass front and rear spars and fiberglass ribs to which fiberglass skins were bonded. To prevent buckling, half-inch thick foam plastic panels were bonded to the interior of the skins between the ribs and spars. Measured bending and twist slopes about the elastic axis were used to determine EI and GJ distributions.

ARW-2

The second DAST aeroelastic research wing is of high-aspect-ratio (10.3) and has supercritical airfoil sections. Its planform is similar to that considered optimum for an energy efficient transport. The structure consists of aluminum spars located at the 25 and 62 percent

3

chord lines, fiberglass skin panels riveted and bonded to the spars, and leading and trailing edges that are attached with screws. The wings are attached to the fuselage with a nearly rigid aluminum carry-through center section. A stress analysis has been performed to determine an elastic axis and EI and GJ distributions.

Results

Transport Wing Model

Figure 5 shows the computed load distribution on the flexible transport wing model at five percent semispan intervals for the design condition. The wing is primarily aft-loaded, with small positive loading at the leading edge out to approximately the 70 percent semispan station. Outboard of this station, the load is negative near the leading edge and positive toward the trailing edge. Calculated deflections along the elastic axis and streamwise twist angles due to aeroelastic deflection, along with the tip deflections and twists observed during a wind tunnel test of the model,[12] are shown in figure 6. The calculated twists were determined by dividing the differences in leading and trailing edge deflection by the local chords. The experimental twists were measured optically with a cathetometer. Agreement between the calculated deflections and twist angles and those observed during the wind tunnel test is very good. The observed tip twist is only slightly larger than the calculated value. Contours of constant deflection, presented in figure 7, show that the wing deformation is composed primarily of bending of the elastic axis. It is well known that bending of a sweptback wing results in washout along the semispan i.e., negative induced twist angles (figure 6b). Torsional deformations are relatively small and increase along the semispan as evidenced by the change in angle, from root to tip, between the deflection contours and the elastic axis.

These results are very similar to those, for the same wing, presented in reference 9 which were calculated with small disturbance aerodynamics. To place this comparison in proper context, however, it is observed that (1) small disturbance theory should yield its best results near design conditions where perturbations are not large and shocks are weak and (2) when using small disturbance theory, pressure differences, which cause structural deformations, are expected to be computed more accurately than actual surface pressures. At off-design conditions, where perturbations may be large, methods which use full potential aerodynamics should more accurately predict structural deformations and surface pressures.

Figure 8 shows twist angles calculated with the present method at a high dynamic pressure. Also shown for comparison are the tip twist measured during the wind tunnel test, and tip twists presented in reference 9, which were obtained using small disturbance aerodynamics, with and without viscous corrections, and also with an initial inviscid full potential calculation.[9] In this case, the use of small

disturbance aerodynamics, even with viscous corrections, results in calculated tip twists that are less accurate than those obtained with inviscid full potential theory. The tip twist determined using the present analysis is nearer to the measured value than that obtained by Chipman et al. using full potential aerodynamic loads. Because of the limited size of the measured structural influence coefficient matrix used in reference 9, wing deformations were computed at relatively few spanwise locations and interpolated to the desired locations. The closer agreement of the present result and experimental data is possibly because the deflections were calculated directly at many more wing locations. Including viscous correction in the small disturbance load calculations resulted in a more accurate predicted tip twist angle (figure 8). This suggests that at high q, incorporating viscous effects in the present analysis should lead to a calculated tip twist that is very near the measured value.

The calculated load distribution at the higher dynamic pressure is shown in figure 9. At outboard stations, there are large negative loads on the forward part of the wing due to high suction pressures ahead of a strong shock near the lower surface leading edge. To illustrate this loading more clearly the surface pressure distribution at the 90 percent semispan station is shown in figure 10. The high suction pressure on the lower surface is quite prominent.

The calculations required to analyze the transport wing are shown in Table I. Computational requirements are listed in terms of the number of iterations, on the fine grid, of the aerodynamic solution required to obtain a converged solution. While no rigid-wing results are presented in this paper, the number of iterations required to perform a rigid-wing analysis is listed to illustrate the additional computations required for the flexible-wing analyses. The additional computations, 40 percent for the design case and 56 percent for the off-design case, are reasonable for the improved results obtained from the flexible wing analyses.

ARW-2

Transonic aerodynamic loads on the ARW-2 wing were calculated at the design cruise conditions, M = 0.80, q = 126.4 psf. Comparisons of lifting pressures and actual surface pressures calculated assuming rigid and flexible wings at constant α and at the ARW-2 design cruise C_L are among the results that are presented. Since fuselage effects cannot be calculated using FLO22, fuselage lift and aerodynamic interference were neglected in this analysis. The DAST ARW-2 configuration has a design cruise C_L of 0.53. An estimated stabilizer trim angle of -4.2^0 and a stabilizer lift-curve slope of 0.012 were used to determine a cruise trim C_L of 0.58 for the wing. Because ARW-2 is joined to the DAST vehicle with a nearly rigid carry-through center section, cambering of the wing due to fuselage deflection was assumed to be negligible. Therefore, it was considered

reasonable to analyze the ARW-2 wing in its free flight trim condition as a flexible, cantilevered wing with its root angle-of-attack chosen such that $C_L = 0.58$. Wind tunnel data which was modified by a FLEXSTAB analysis was used to determine an estimated wing trim α of 1.36°. In the present inviscid analysis, however, the design trim C_L was obtained at $\alpha = 0.91^\circ$ for the flexible wing and $\alpha = 0^\circ$ for the rigid wing.

Figure 11 shows calculated rigid-wing and flexible-wing lift and pitching moment (C_M) coefficients for a range of angles-of-attack at $M = 0.80$, $q = 126.4$ psf. As expected, the inclusion of flexibility effects in the analysis results in considerable load relief on the wing. The calculated spanwise lift distributions shown in figure 12 illustrate the loss of lift due to aeroelastic deformations at $\alpha = 1.36^\circ$. In this case, including aeroelastic effects in the wing analysis resulted in a 20 percent reduction in the calculated lift. The effects of wing flexibility on the nondimensional lifting pressure (ΔC_p) distributions is shown in figure 13 at intervals of five percent semispan. The rigid-wing pressure distribution (figure 13a) is characterized by a strong upper surface shock along the entire semispan, as evidenced by the humps in the ΔC_p distributions, and relatively high lift near the leading edge. When flexibility effects are included in the analysis, the shock moves forward and weakens inboard of approximately the 50 percent semispan station and outboard of the 80 percent semispan station and completely disappears between the 50 percent and 80 percent stations (figure 13b). A comparison of rigid-wing and flexible-wing pressure distributions at the 90 percent semispan location (figure 14) shows in detail the effects of aeroelastic deformations on surface pressures and on shock strength and location. Aft of 70 percent chord, however, the pressure distribution is virtually unchanged.

Results of the analysis of ARW-2 at $C_L = 0.58$ are presented in figures 15-18. Calculated spanwise lift distributions on the rigid wing at $\alpha = 0^\circ$ and the flexible wing at $\alpha = 0.91^\circ$ (figure 15) show how the lift is shifted inboard on the flexible wing. Figure 16 shows the load distributions at intervals of five percent semispan. The more pronounced effects are seen at the outboard stations where, near the leading edge, the lift on the flexible wing is significantly less than that on the rigid wing. This is due to the smaller suction pressure at the upper surface leading edge caused by a decrease in the local angle-of-attack. A plot of surface pressures at the 90 percent station (figure 17) shows that aeroelastic effects cause the upper surface shock to weaken and move forward and the suction peak to decrease by about 18 percent. However, the pressure distribution on the aft 30 percent of chord is unchanged. As in the case of the transport wing model, at the ARW-2 design C_L, bending of the elastic axis accounts for most of the wing deflection (figure 18).

The number of fine-grid iterations of the aerodynamic solution required to analyze ARW-2

are presented in Table II. The rigid-wing analysis at $\alpha = 1.36^\circ$ required more fine grid iterations than the corresponding flexible wing analysis because very few calculations were made on the two coarser grids before doing the fine grid calculations. This slowed convergence of the fine grid solution. A more representative example is the 100 fine grid iterations required for the rigid wing analysis at 0°, in which substantially more calculations were made on the coarser grids to increase the rate of convergence. Using 100 as the number of fine grid iterations required to obtain a rigid-wing solution, the flexible-wing solutions for $\alpha = 0.91^\circ$ and 1.36° require 15 percent and 35 percent more iterations, respectively. The additional cost of these calcuations is quite reasonable.

Concluding Remarks

A method for calculating steady transonic loads on flexible wings has been developed by combining a nonlinear full potential flow analysis with a linear structural analysis. The structural model is not limited by the assumptions of beam theory. Because of the type of structural information that was available, however, the present method was used in a beam analysis mode to analyze two high-aspect-ratio swept wings - a wind tunnel flutter model of a proposed executive-jet transport wing and the DAST (Drones for Aerodynamic and Structural Testing) ARW-2 (Aeroelastic Research Wing Number 2). At design conditions where flow perturbations are relatively small and shock waves are weak, calculated twist angles and deflections of the tranport wing model show good agreement with measured data and with previously published results obtained using transonic small disturbance aerodynamics. At off-design conditions, however, where perturbations are larger and shocks are stronger, results determined using full potential aerodynamics were shown to be more accurate than those based on small disturbance theory.

Results for the transport wing model at an off-design condition indicate that the ability to model the wing and its loading as a desired array of area elements and discrete loads, as in the present structural analysis, can lead to increased accuracy of the computed aeroelastic deformations. For the two wings studied in this investigation, aeroelastic effects on the load distributions at design conditions were primarily due to bending deflections. These bending deflections of swept wings induced negative streamwise twist angles and the resulting changes in calculated loads.

The flexible wing analyses presented in this paper required from 15 to 56 percent more computations than the corresponding rigid-wing analyses. Even with the increased computing requirements, the costs of the flexible wing analyses were still quite reasonable.

References

[1]Mason, W. H.; MacKenzie, D.; Stern, W.; Ballhaus, W. F.; and Frick, J.: An Automated Procedure for Computing the Three Dimensional Transonic Flow over Wing-Body Combinations, Including Viscous Effects. Volume I - Description of Analysis Methods and Applications, AFFDL-TR-77-122, Volume I, February 1977.

[2]Jameson, A.; and Caughey, D. A.: Numerical Calculation of the Transonic Flow Past a Swept Wing, NASA CR-153297, 1977.

[3]Boppe, C. W.: Calculation of Transonic Wing Flows by Grid Embedding, AIAA Paper 77-207, Presented at the AIAA 15th Aerospace Sciences Meeting, Los Angeles, CA, January 1977.

[4]Bisplinghoff, R. L.; Ashley, H.; and Halfman, R. L.: Aeroelasticity, Addison-Wesley Publishing Co., Inc., Reading, MA, 1957.

[5]Pai, S. I.; and Sears, W. R.: Some Aeroelastic Properties of Swept Wings, Journal of the Aeronautical Sciences, Vol. 16, No. 2, February 1949.

[6]Tinoco, E. N.; and Mercer, J. E.: FLEXSTAB - A Summary of the Functions and Capabilities of the NASA Flexible Airplane Analysis Computer System, NASA CR-2564, 1974.

[7]Nelson, D. W.; Gornstein, R. J.; and Dornfeld, G. M.: Prediction of Maneuvering Drag Polars Including Elasticity Effects for AFTI-F111, AIAA Paper 81-1658, Presented at the AIAA Aircraft Systems and Technology Conference, Dayton, OH, August 1981.

[8]Rogers, W. A.; Braymen, W. W.; and Shirk, M. H.: Design, Analyses, and Model Tests of an Aeroelastically Tailored Lifting Surface, AIAA Paper 81-1673, Presented at the AIAA Aircraft Systems and Technology Conference, Dayton, OH, August 1981.

[9]Chipman, R.; Waters, C.; and MacKenzie, D.: Numerical Computation of Aeroelastically Corrected Transonic Loads, AIAA Paper 79-0766, Presented at the AIAA/ASME/ASCE/AHS 20th Structures, Structural Dynamics and Materials Conference, St. Louis, MO, April 1979.

[10]Ruhlin, C. L.; Rauch, F. J.; and Waters, C.: Transonic Flutter Study of a Wind-Tunnel Model of a Supercritical Wing with/without Winglet, AIAA Paper 82-0721, Presented at the AIAA/ASME/ASCE/AHS 23rd Structures, Structural Dynamics and Materials Conference, New Orleans, LA, May 1982.

[11]Murrow, H. N.; and Eckstrom, C. V.: Drones for Aerodynamic and Structural Testing (DAST) - A Status Report, Journal of Aircraft, Vol. 16, No. 8, pp. 521-526, August 1979.

[12]Rauch, F. J.; and Waters, C.: Analyses and Initial Tests Conducted on a 1/6.5 Size Flutter Model of an Executive-Jet Transport Supercritical Wing with/without Winglet, NASA CR-165857, November 1978.

TABLE I.   COMPUTATIONS REQUIRED TO ANALYZE TRANSPORT WING MODEL

Structure	Flow Conditions	Aerodynamic Iterations
Rigid	Design Cruise	90
Flexible	Design Cruise	125
Flexible	High q	140

TABLE II.   COMPUTATIONS REQUIRED TO ANALYZE ARW-2

Structure	Flow Conditions	Aerodynamic Iterations
Rigid	Design Cruise, $\alpha = 1.36^0$	190
Flexible	Design Cruise, $\alpha = 1.36^0$	135
Rigid	Design Cruise, $\alpha = 0^0$	100
Flexible	Design Cruise, $\alpha = 0.91^0$	115
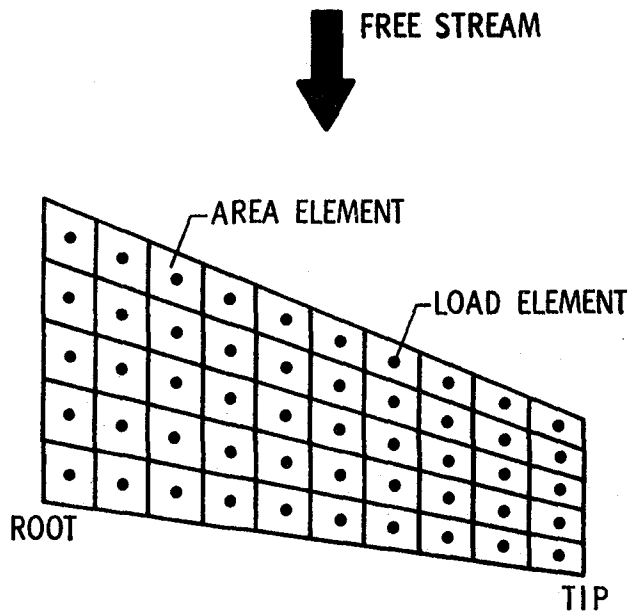
Fig. 1 Load discretization.

Fig. 2 Reference axes and representation of load element.

Fig. 3 Aerodynamic/structural iteration process.
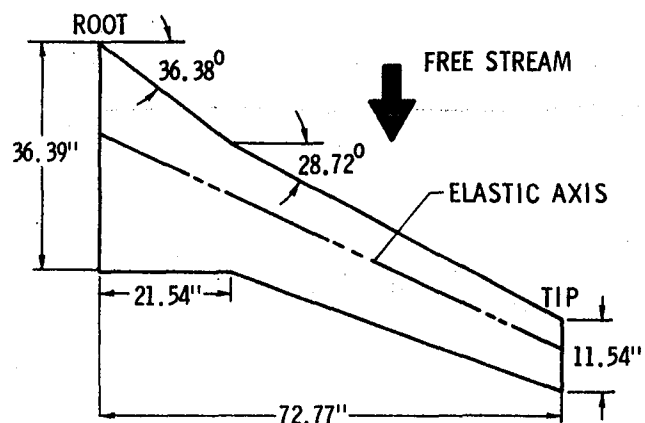
(a) Transport wing model
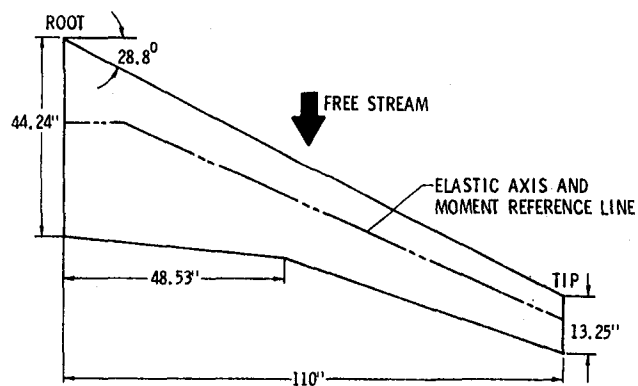
(b) ARW-2

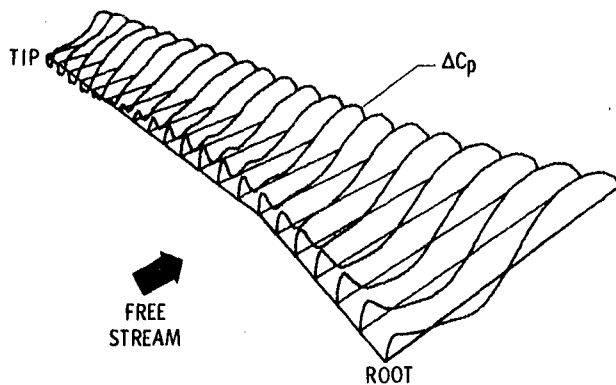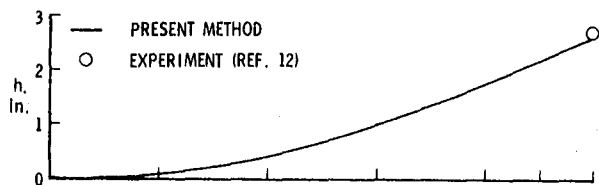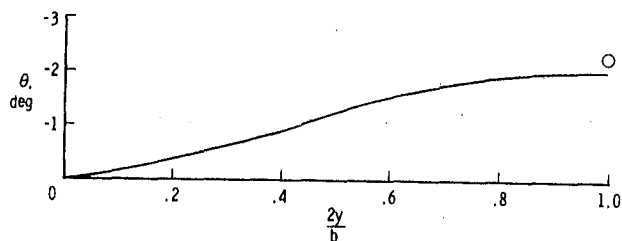Fig. 4 Planforms of wings analyzed in present study (dimensions in inches).

Fig. 5 Nondimensional loading on transport wing model at M = 0.82, q = 30 psf.

(a) Deflections

(b) Streamwise twist angles

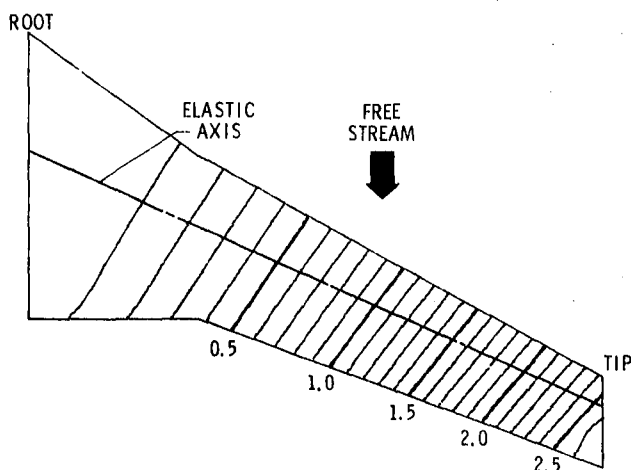Fig. 6 Deflections and streamwise twists of transport wing model at M = 0.82, q = 30 psf.

Fig. 7 Contours of constant deflection (in inches) of transport wing model at M = 0.82, q = 30 psf.
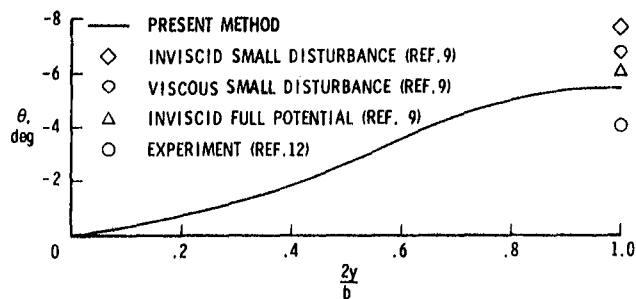
Fig. 8 Streamwise twists of transport wing model at M = 0.82, C_L = 0.11.
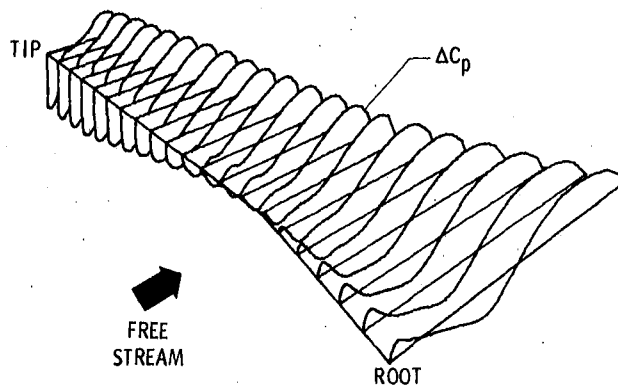
Fig. 9 Nondimensional loading on transport wing model at M = 0.82, C_L = 0.11.
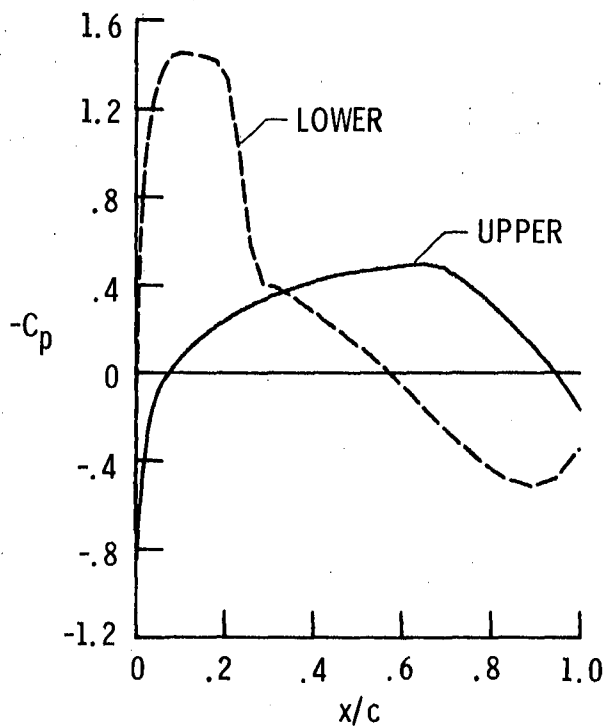
Fig. 10 Nondimensional pressures on transport wing model at $\frac{2y}{b}$ = 0.90, and at M = 0.82, C_L = 0.11.

8
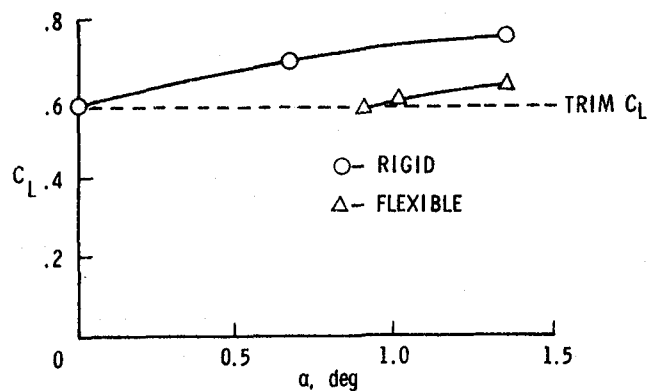
(a) Lift coefficients
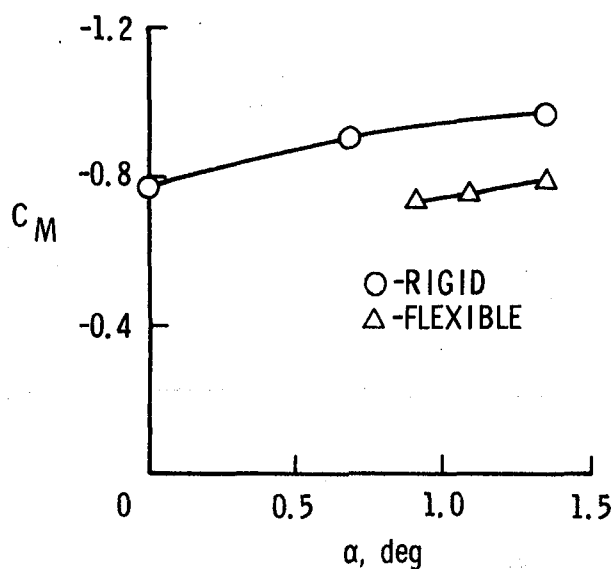
(a) Rigid wing

(b) Pitching moment coefficients

Fig. 11 ARW-2 rigid-wing and flexible-wing lift and pitching moment coefficients at M = 0.80, q =126.4 psf.
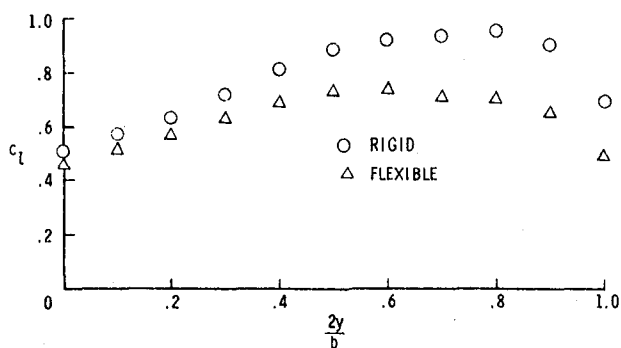
(b) Flexible wing

Fig. 13 Nondimensional loading on ARW-2 at M = 0.80, α = 1.36°, q = 126.4 psf.

Fig. 12 Spanwise lift distributions on rigid and flexible ARW-2 at M = 0.80, α = 1.36°, q = 126.4 psf.
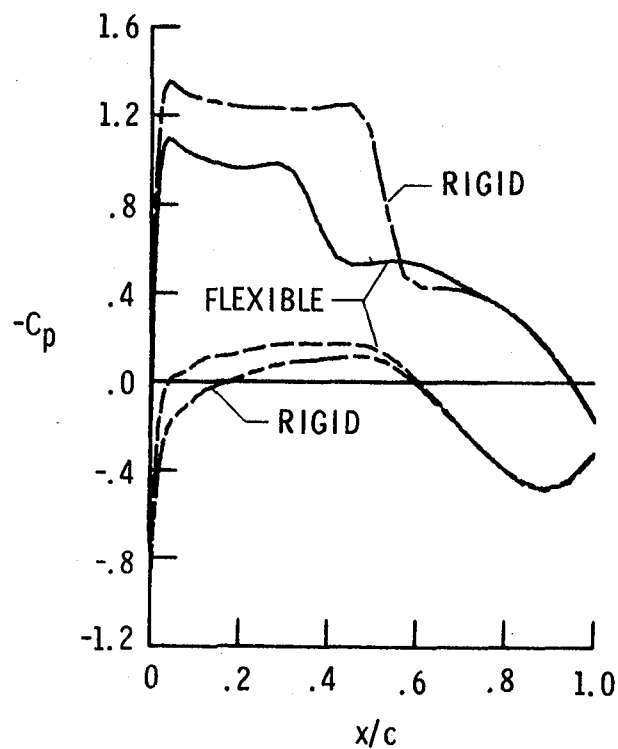
Fig. 14 Nondimensional pressures on rigid and flexible ARW-2 at $\frac{2y}{b}$ = 0.90 and at M = 0.80, α = 1.36°, q = 126.4 psf.
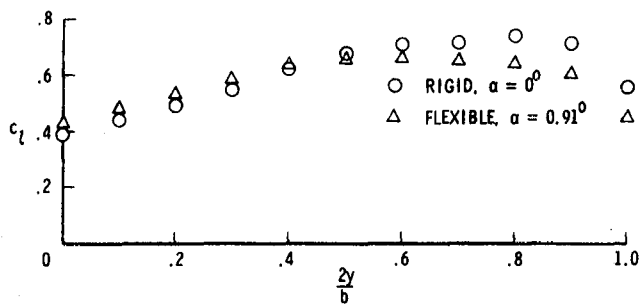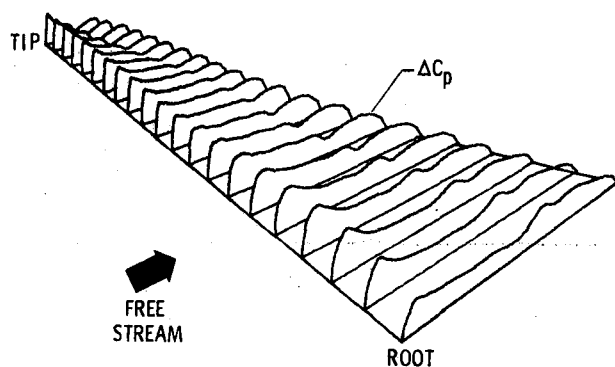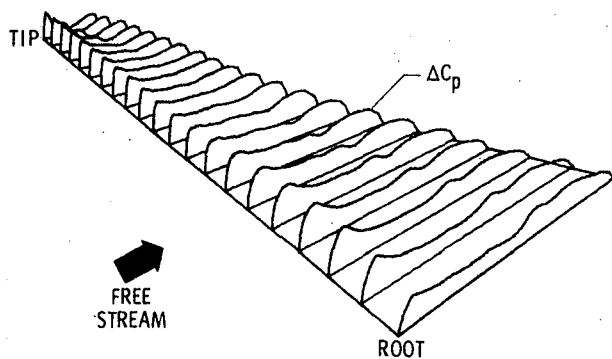
Fig. 15 Spanwise lift distributions on rigid and flexible ARW-2 at M = 0.80, C_L = 0.58, q = 126.4 psf.

(a) Rigid wing (α = 0°)

(b) Flexible wing (α = 0.91°)

Fig. 16 Nondimensional loading on ARW-2 at M = 0.80, C_L = 0.58, q = 126.4 psf.
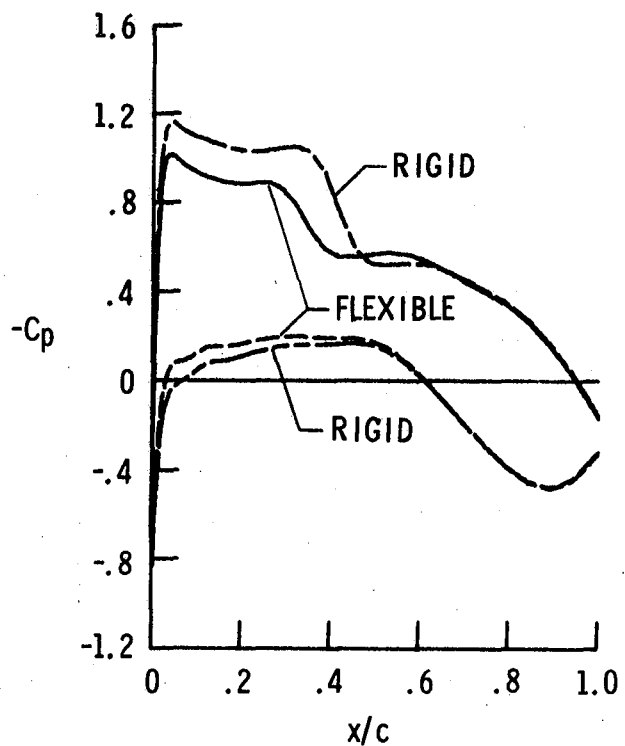

Fig. 17 Nondimensional pressures on rigid and flexible ARW-2 at $\frac{2y}{b}$ = 0.90 and at M = 0.80, C_L = 0.58, q = 126.4 psf.
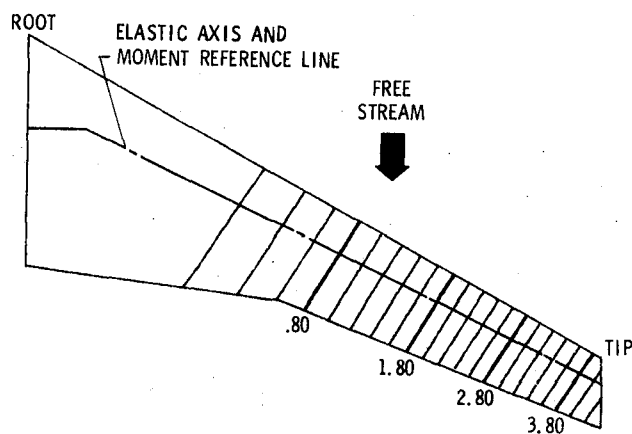

Fig. 18 Contours of constant deflection (in inches) of ARW-2 at M = 0.82, C_L = 0.58, q = 126.4 psf.

1. Report No. NASA TM 83296	2. Government Accession No.	3. Recipient's Catalog No.
4. Title and Subtitle Application of a Transonic Potential Flow Code to the Static Aeroelastic Analysis of Three-Dimensional Wings		5. Report Date April 1982
		6. Performing Organization Code 2250
7. Author(s) Woodrow Whitlow, Jr. and Robert M. Bennett		8. Performing Organization Report No.
		10. Work Unit No. 505-33-53-07
9. Performing Organization Name and Address NASA Langley Research Center Hampton, VA 23665		11. Contract or Grant No.
		13. Type of Report and Period Covered Technical Memorandum
12. Sponsoring Agency Name and Address National Aeronautics and Space Administration Washington, DC 20546		14. Sponsoring Agency Code

15. Supplementary Notes

This paper was presented at the AIAA/ASME/ASCE/AHS 23rd Structures, Structural Dynamics and Materials Conference, May 10-12, 1982, New Orleans, Louisiana, AIAA Paper No. 82-0689.

16. Abstract

A method for including elastic effects in steady, transonic wing analysis is presented. Since the aerodynamic theory is nonlinear, the method requires the coupling of two iterative processes - an aerodynamic analysis and a structural analysis. A full potential analysis code, FLO22, is combined with a linear structural analysis to yield aerodynamic load distributions on and deflections of elastic wings. This method was used to analyze an aeroelastically-scaled wind tunnel model of a proposed executive-jet transport wing and an aeroelastic research wing. The results are compared with the corresponding rigid-wing analyses, and some effects of elasticity on the aerodynamic loading are noted.

17. Key Words (Suggested by Author(s)) Three-Dimensional Transonics Steady Full Potential Static Aeroelasticity Linear Structural Analysis	18. Distribution Statement Unclassified - Unlimited Subject Category 02

19. Security Classif. (of this report) Unclassified	20. Security Classif. (of this page) Unclassified	21. No. of Pages 12	22. Price A01